



# Spatio-temporal analysis of changes occurring in land use and its impact on land surface temperature

Tanushri Jaiswal<sup>1</sup> · Dalchand Jhariya<sup>1</sup> · Surjeet Singh<sup>1</sup>

Received: 28 September 2022 / Accepted: 10 March 2023 / Published online: 31 March 2023  
© The Author(s), under exclusive licence to Springer-Verlag GmbH Germany, part of Springer Nature 2023

## Abstract

This study shows how remote sensing and Geographic Information System (GIS) can extract land surface temperature (LST) from the Landsat 5, 7, and 8 datasets. In this research, LST over Kharun's lower catchment, located in Chhattisgarh, India, has been estimated. LST data from 2000, 2006, 2011, 2016, and 2021 were analyzed to see how the LULC pattern changed and how that changed LST. In 2000, the average temperature of the study region was 27.73 °C, whereas in 2021, it reached 33.47 °C. When the average temperature values for each class were determined, it was discovered that forest and adjacent waterbodies had the lowest values, with about 24.15 °C in 2000 and 27.65 °C in 2021, whereas urban regions had more variation in values, ranging from 30.15 °C in 2000 to 38.95 °C in 2021. There could be an increase in LST over time because cities are replacing the green cover. For example, there was a notable increase of 5.74 °C in the mean LST over the research area. The findings revealed that places with extensive urban sprawl had LST between 26 and 45°, which was greater than other natural land cover types, such as vegetation and waterbodies, which was between 24 and 35°. These findings support the suggested method's effectiveness for retrieving LST from the Landsat 5, 7, and 8 thermal bands when combined with integrated GIS approaches. So, the goal of this study is to look at Land Use Change (LUC) and changes in LST using Landsat data and figure out how they are related to LST, the Normalized Difference Vegetation Index (NDVI), and the Normalized Built-up Index (NDBI), which are used as major components.

**Keywords** LULC · LST · NDVI · NDBI · GIS · Kharun

## Introduction

Rapid urbanization results from a rising global population and the subsequent migration of people in rural areas to cities (Farid et al. 2022; Moss and Neill 2012). Analysts in the twenty-first century have paid more attention to the environmental effects of urbanization (Fonseka et al. 2019; Spence et al. 2009). Since 1990, the percentage of urban residents has increased dramatically; according to remotely sensed data, almost 50% of the world's population now resides in urban areas (Farid et al. 2022; Fonseka et al. 2019). Whether it is in a developed nation or a developing one, the rapid growth of cities is making it

hard to create prosperous and environmentally friendly cities. The situation is getting worse because urbanization is becoming more linked to the estimated climate change, which is the most important environmental event of this century (Mohammad and Goswami 2019; Fonseka et al. 2019). For example, a city's climate is different from that of the rural areas around it (Chen et al. 2006; Ding and Shi 2013; Hamdi 2010). Most urban land use changes are caused by the reduction of natural vegetation and land cover by displacing it with impermeable urban materials, which results in variations of temperature at the earth's surface (Lo and Quattrochi 2003; Fu and Weng 2016).

Over the past decade, researchers have focused more on local and regional climates affected by human activities in an effort to determine the causes of the rapid changes occurring to the global weather (Adegoke et al. 2003; Ibrahim 2017). Increasing industry and urbanization is a major contributor to global warming. Growth can be seen in these sectors, including industries, hospitals, and residential areas. However, due to these changing conditions, a drastic change in land cover can also be seen (Jiang and Tiang 2010; Kayet et al. 2016;

---

Responsible Editor: Philippe Garrigues

---

✉ Tanushri Jaiswal  
tanushrijaiswal01@gmail.com

<sup>1</sup> Department of Applied Geology, National Institute of Technology Raipur, G.E. Road, Raipur, Chhattisgarh 492 010, India

Idowu et al. 2019). While we cannot stop global warming, we can slow it down by improving management. Numerous researchers have examined these adverse effects of progress in various domains like water, land, and air quality and have provided their findings (McGrane 2016; Salereno 2018) but there is a need of more research related to the impact of urbanization in form of luck to be done in the newly formed cities, or district which are still in their developing phase. A time to time study should be done in such areas so that changes can be assessed and suitable measures for development can be done in a planned way. As Raipur is also a newly formed district and the area around its vicinity is actively developing, therefore study area has been selected for the study purpose.

LUC and associated changes are known to be the primary aspects to be considered for achieving sustainable development and are extremely significant for managing and monitoring of natural resources (Sinha et al. 2015). For this reason, urban planners need to maintain track of changes in land use using up-to-date data and forward-looking strategies (Herold et al. 2003). Remote sensing is a very advanced method that uses a combination of high-resolution images and image processing techniques to show how land use is changing (Chaudhuri and Mishra 2016; Karakuş 2019; Shukla et al. 2021). With the help of different techniques, remote sensing has been used to map LULC and study changes (Butt et al. 2015; Liu and Yang 2015). It was said that Landsat satellite images are useful for LULC changes and also for analyzing urban regions (Karakuş 2019). A number of studies have established connections between LULC shifts and urban temperature patterns (Chen et al. 2006; Karakuş 2019; Reynolds et al. 2008; Weng et al. 2004; Zheng et al. 2014). Remote sensing data is also used to measure the amount of energy reflected in the Red and near infrared parts of the electromagnetic spectrum. This information can be used to quantify urban vegetation and analyze occurred changes (Gorgani et al. 2013; Jeevalakshmi et al. 2016; Yue et al. 2007). Land surface temperature (LST) is one of the most important parts of the physics of land surface processes, which include interactions between the surface and the atmosphere and the flow of energy between the ground and the atmosphere. Most of the time, places with high NDVI have the lowest LSTs. This negative relationship between NDVI and LST is useful for studying the weather in cities (Gorgani et al. 2013; Guha et al. 2018; Yuan and Bauer 2007). It has also been observed by many researchers that vegetated and watered landscapes are cooler than urban areas (Gorgani et al. 2013; Joshi and Bhatt 2012). In addition, the LST–NDBI was also quantitatively interpreted using linear regression method at pixel level. A strong correlation (0.71 and 0.61) with the NDBI has been found at urbanized area with lesser vegetation representing the Urban Heat Island (UHI) effect whereas correlation gets weaker for urban areas mixed with cultivation and vegetation area. It could be

attributable to the presence of natural landscapes within the urban region (Guha et al. 2018).

Hence, work is aimed to estimate the variation in LULC and its effects on LST over the past 20 years on the nearby environment in terms of temperature variation which were then validated with the Moderate Resolution Imaging Spectroradiometer (MODIS) LST products using the SW algorithm (Aik et al. 2020; Mukherjee et al. 2014; Nikam et al. 2016; Srivastava et al. 2009). Attempts have been made to integrate remote sensing (RS) and GIS techniques based on other pieces of literature in the current study. The research can examine the combined effects of temperature and LULC changes on the study area (Feizizadeh et al. 2013; Tsou et al. 2017; Nayak and Mandal 2019; Gohain et al. 2021). For the study, Landsat images for the relevant years were downloaded from the United States Geological Survey (USGS). These images are available freely throughout longest temporal range; such type of studies is very important to be performed at regular intervals in order to see the rate of urban growth and its impacts to the environment (Rajeshwari and Mani 2014; Alhawiti and Mitsova 2016). The chosen imagery was from Landsat TM, ETM, and Landsat 8 OLI (Basu and Das 2023). Kharun's lower catchment has been chosen for the approaches implications since the part combination of urban and rural sprawl and cultivation and vegetation cover. This region has been selected to highlight the changes in the area with greater urban sprawl than that of remote rural areas (Tsou et al. 2017 and Zhang et al. 2017).

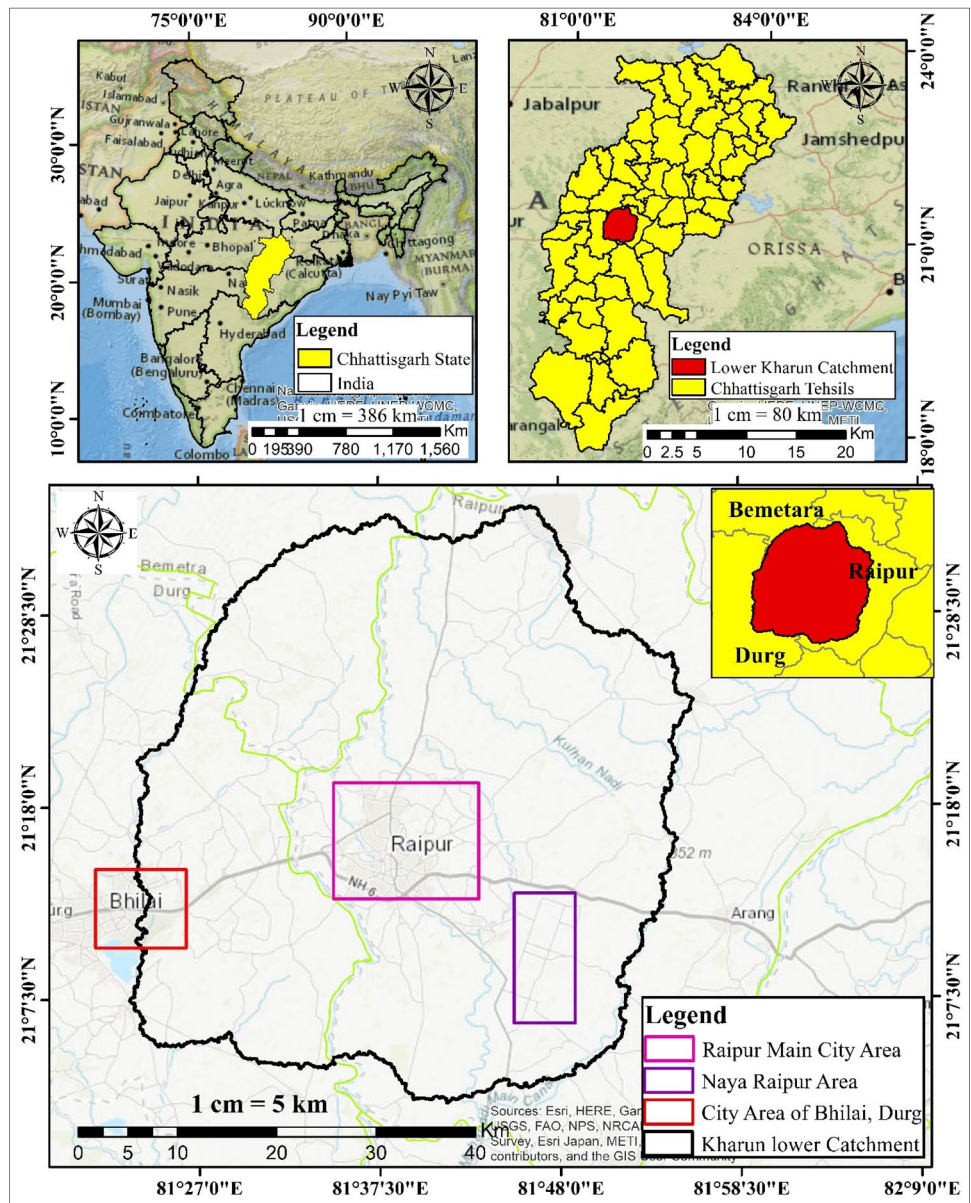
One of the leading causes of climate change is LULC which has its impact on LST as well. Therefore, observed changes that occurred in the LULC have been assessed to see its effects on surface temperature (Feizizadeh et al. 2013; How Jin Aik et al. 2020) for Chhattisgarh's Kharun lower catchment; this research aimed to investigate the effects of LULC on surface temperature and to see the correlation of LST with NDVI and NDBI. In addition, a spatio-temporal analysis of the research region was conducted. The data reveal that areas covered by vegetation or waterbodies have remained essentially constant, while the urban region and its surroundings are experiencing extreme heat stress.

## Study area

The study area covers the central portion of Raipur and Durg Districts and some parts of Bemetara District, as shown in Fig. 1. A significant amount of study area comes under Raipur, which is the most developed district and also the capital of Chhattisgarh state, with the urbanized city area of the district covered under it. At the same time, the site also has some extended city part of Durg district and industrial area coming under it, which makes the space suitable for the study purpose.

Kharun River is a tributary of Seonath and is one of the principal rivers of Raipur and Durg; the Lower Kharun Catchment (LKC) covers a total area of about 2541.81Sq.

**Fig. 1** Location of the study area in reference to India



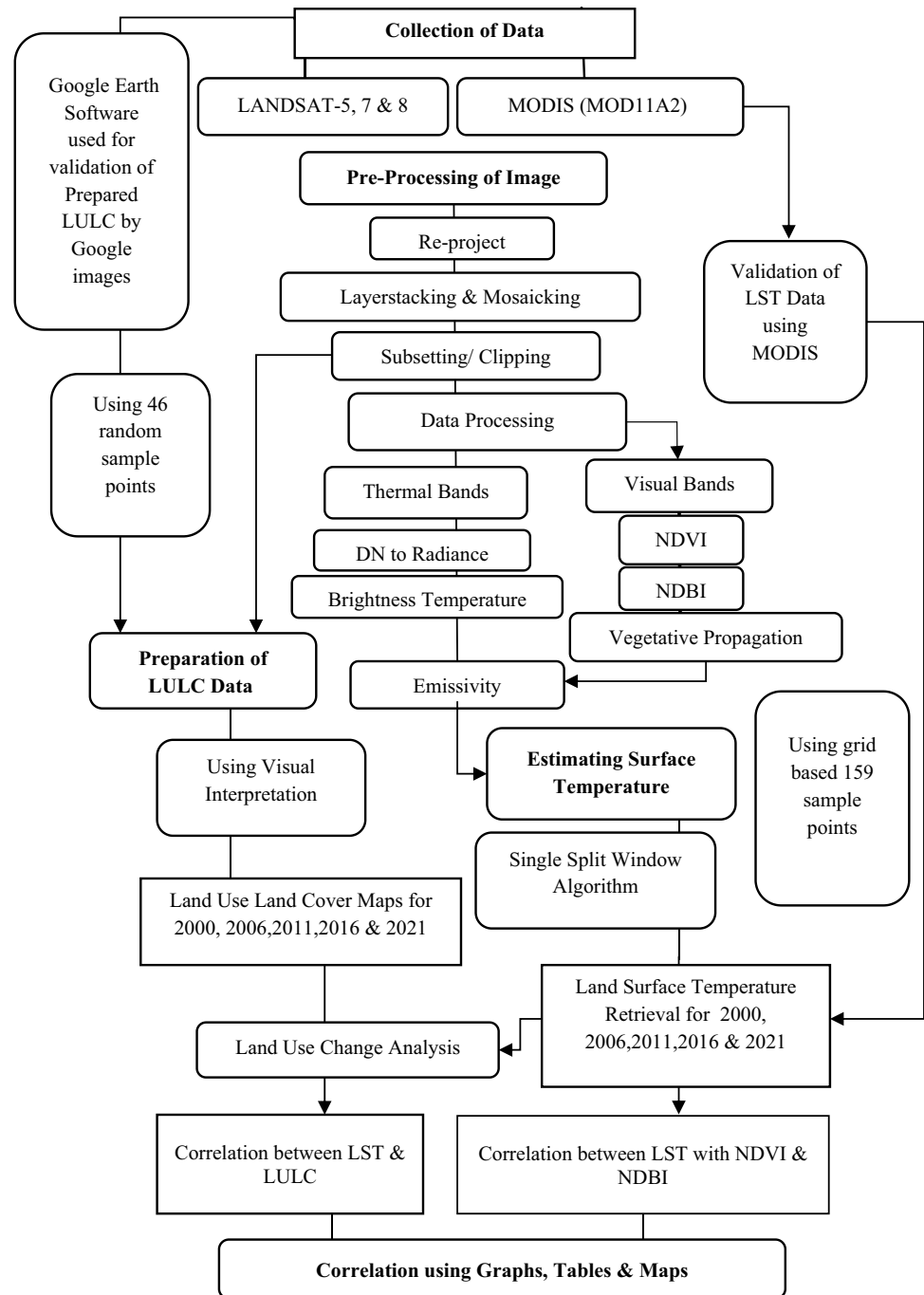
Km. The catchment covers the entire settlement area of Raipur District and part of urban area of Durg district hence considered to be among highly populated catchment in the state. The whole catchment has diverse land use with a significant portion of the area covered by agricultural land, a few patches of vegetation, and number of waterbodies, and the central part of the basin has urban land, including an industrial area, while a rural area is distributed in small patches throughout the basin area.

**Climate type**

LKC is situated in the plain area of Chhattisgarh with basically three seasons, starting with the summer, which occurs from middle of February to middle of June, proceeding with

the monsoon from Mid-June to Mid-October and finally winter season, which begins in middle of October and extends till Mid-February. LKC has a moderate type of climate except for the summer season, when the weather is extremely hot, with temperatures exceeding to almost 46°C during the day in the hottest month of May and during the month of January with a minimum recorded temperature of 9°C. Overall catchment has tropically dry to humid type of climate with an average rainfall of about 1200mm (Kumar et al. 2017). Monsoon is prevailed by the southwest winds, with a major part of rainfall occurring in the month of July to August. In accordance with the long-term rainfall data for the Kharun Basin, the five successive months from June to October constitute nearly 90% of all rainfall. On a smaller scale, droughts recur every 3 to 4 years (Sinha et al. 2013).

Fig. 2 Applied methodologies



LKC is divided into seven rock types distributed throughout the study area. Maximum area has been covered with stromatolitic dolomitic limestone, shale comes in second, and stromatolitic dolomitic limestone along with sandstone is at the central part of the basin. Fourth is the argillaceous ferruginous sandstone and the rest stromatolitic dolomitic limestone, shale with sandstone, and laterite is distributed in small patches all over the area (Lithology data, Bhukosh). Three major soil types are found in

the basin: Deep Black Soil covering more than 60% of the total area, while the rest is divided into Medium Black Soil and Laterite Soil (source: NBSSLUP, Nagpur). Soil type and its composition have a direct impact on land surface temperature (LST), and significant correlations were found between soil characteristics and elevation, LST, and reflectance (Sayão et al. 2018, 2020; Srivastava et al. 2010) by different researchers.



**Table 1** Details of data used

| S. No | Data used  | Spatial resolution | Path and row                     | Data description  | Source  |
|-------|--|--------------------|----------------------------------|---|---|
| 1     | Landsat 5 Thematic Mapper (TM)   |                    | 142 and 45                       | LT05_L1TP_142045_20060428   | <a href="https://earthexplorer.usgs.gov/">https://earthexplorer.usgs.gov/</a> |
|       | Other bands  | 30m                |                                  | _20161122_01_T1   |   |
|       | Thermal Band-6 (1 and II)  | 120m               |                                  | and<br>LT05_L1TP_142045_20110426<br>_20161208_01_T1<br>(Used for years 2006 and 2011) |   |
| 1     | Landsat 7 Enhanced Thematic Mapper (ETM)                                     |                    | 142 and 45                       | LE07_L1TP_142045_20000403   | <a href="https://earthexplorer.usgs.gov/">https://earthexplorer.usgs.gov/</a> |
|       | Other bands  | 30m                |                                  | _20170212_01_T1<br>(Used for year 2000)   |   |
|       | Thermal Band-6 (1 and II)  | 60 (30)m           |                                  |   |   |
| 2     | Landsat 8  |                    | 142 and 45                       | LC08_L1TP_142045_20160423   | <a href="https://earthexplorer.usgs.gov/">https://earthexplorer.usgs.gov/</a> |
|       | Panchromatic   | 15m                |                                  | _20170326_01_T1   |   |
|       | Operational Land Imager  | 30m                |                                  | and<br>LC08_L1TP_142045_20210405  |   |
|       | Thermal Infrared Sensor (B10 and 11)   | 100m               |                                  | _20210409_01_T1<br>(Used for year 2021)   |   |
| 3     | MOD11A1.v006 Terra Land Surface Temperature and Emis sivity Daily Global 1km |                    |                                  | MOD11A1.A2000094.   | <a href="https://earthexplorer.usgs.gov/">https://earthexplorer.usgs.gov/</a> |
|       |  |                    |                                  | h25v06.006.2015058033317.<br>hdf  |   |
|       |  |                    |                                  | MOD11A1.A2006119.   |   |
|       |  |                    |                                  | h25v06.006.2015289021505.<br>hdf  |   |
|       |  |                    |                                  | MOD11A1.A2011115.   |   |
|       |  |                    |                                  | h25v06.006.2016054125328.<br>hdf  |   |
|       |  |                    | MOD11A1.A2016115.                |   |   |
|       |  |                    | h25v06.006.2016239021309.<br>hdf |   |   |
|       |  |                    | MOD11A1.A2021097.                |   |   |
|       |  |                    | h25v06.006.2021098094642.<br>hdf |   |   |

## Materials and methodology

Here, the GIS platform has processed remotely sensed data to get the desired output; the applied methodology is shown briefly in Fig. 2. Current work has been done using the Landsat data series (Landsat 5, 7, and 8).

Landsat datasets were downloaded from <https://earthexplorer.usgs.gov/> website. Pre-processing of these images including noise correction, mosaicking, and clipping was done initially, proceeding with the further processing part; the first step was preparing the LULC maps for all the 5 years (2000, 2006, 2011, 2016, and 2021) on the False Colour Composite (FCC) images of the respective years using the techniques of visual interpretation. FCC for all the years was prepared from the visible band (Bands 1, 2, 3, and 4 in the case of Landsat 5 and 7 while Bands 2, 3, 4, and 5, for Landsat 8) and was used for the preparation of LULC maps for the all the 5 years considered for the study. After creation of land use map for each year, further processing has been

done for calculating LST from Landsat datasets. Details for the used datasets are given in Table 1.

## Image processing and classification

The image processing softwares (ArcMap & Qgis) were used to create LULC from Landsat 7 data for 2000, Landsat 5 for years 2006 and 2011, and Landsat 8 for 2016 and 2021. Created FCC images were used for Landsat 7, 5, and 8 for visual interpretation and accurate categorization. On the basis of LULC classification given by Anderson (1976), only the first and second levels can be identified in a mid-range resolution but all of the Level 2 categories cannot be interpreted in the same way with accuracy; therefore, Level 1 which are more generic in nature are included in the LULC classification (Anderson 1976). Data was classified into five broad LULC classes (Gupta and Sharma 2020; Kafi et al. 2014; Karakus 2019), including natural vegetation, water, cultivation land, settlement, and open/Barren land (Babalola et al. 2014; Jaber et al. 2022; Verma and Raghubanshi 2019)

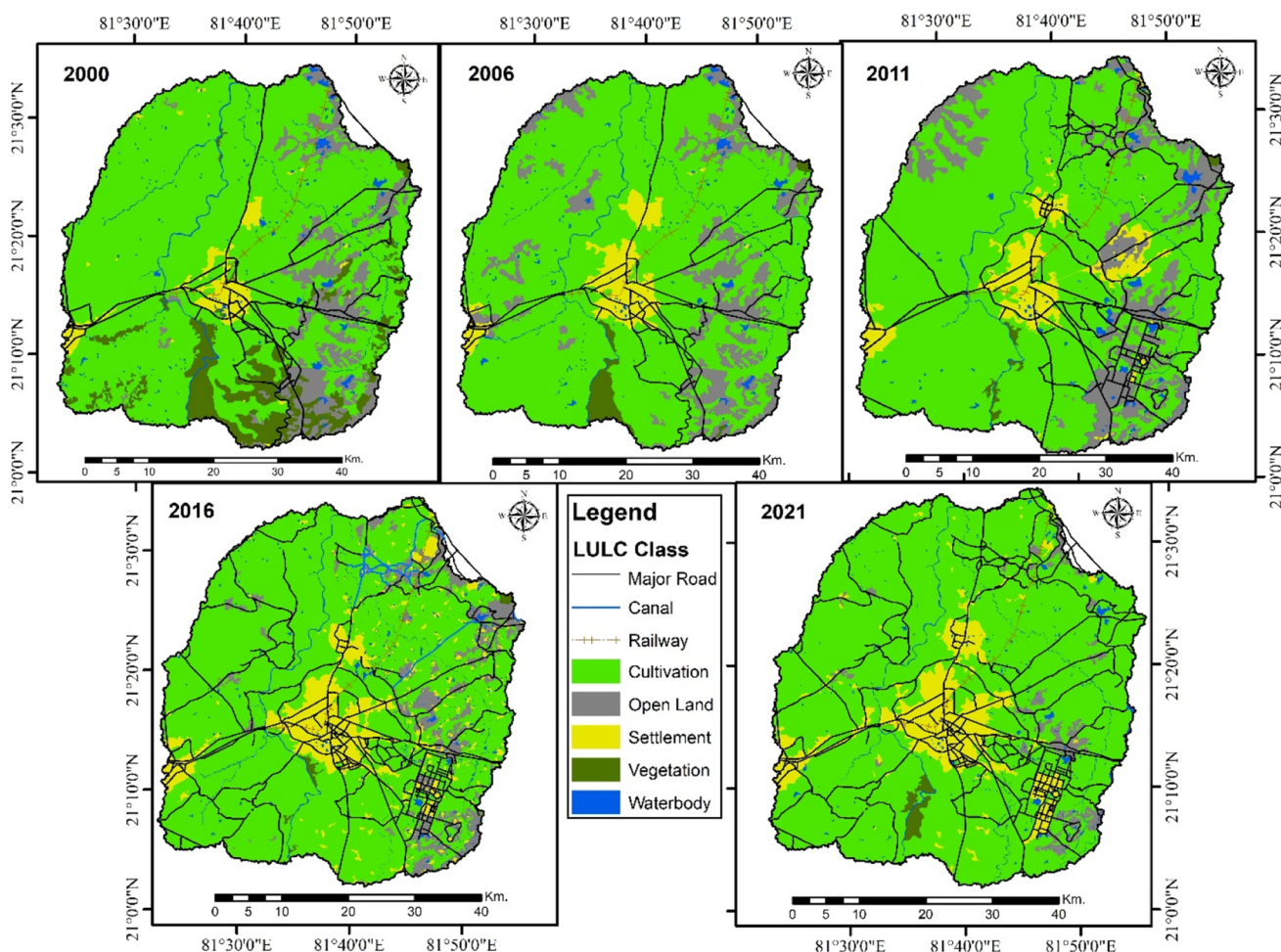


**Fig. 3** LULC from year 2000 to 2021

(see Fig. 3). A visual classification was applied to the image which can provide insight into how land cover has changed over time (Shalaby and Tateishi 2007; Vellaiyan et al. 2017 and Basha et al. 2018; Shalaby and Karakus 2019; Abdalkadhum et al. 2020) (Karakus 2019;).

**Brightness temperature retrieval from the Landsat data series**

Once LULC maps are prepared, work has further proceeded with estimating surface temperature for all the years. LST was derived from the thermal bands of these remote sensing datasets which were used in order to see the impact of LULC on the LST for the study area. The Single Window (SW) algorithm was applied for LST computation (Sobrino et al. 2004; Rajeshwari and Mani 2014; Kamran et al. 2015; Alhawiti and Mitsova 2016), which includes several further steps, including conversion of DN

(digital number) to radiance using the Qcal Min and Max values given in the Meta at files from the data directory. After this, Top of Atmosphere (TOA) reflectance values were calculated, proceeding with calculating NDVI values using the Red and NIR (near infrared) bands; after that, Brightness & Emissivity calculation was done, and finally, temperature retrieval.

**Conversion of digital number (DN) to spectral radiance**

First, the DN values of the Landsat images for the thermal infrared band were converted into spectral radiance, which was calculated using the equation below for Landsat 5, 7, and 8 respectively: (Landsat Project Science Office 2002, 2016; Sekertekin et al. 2015):

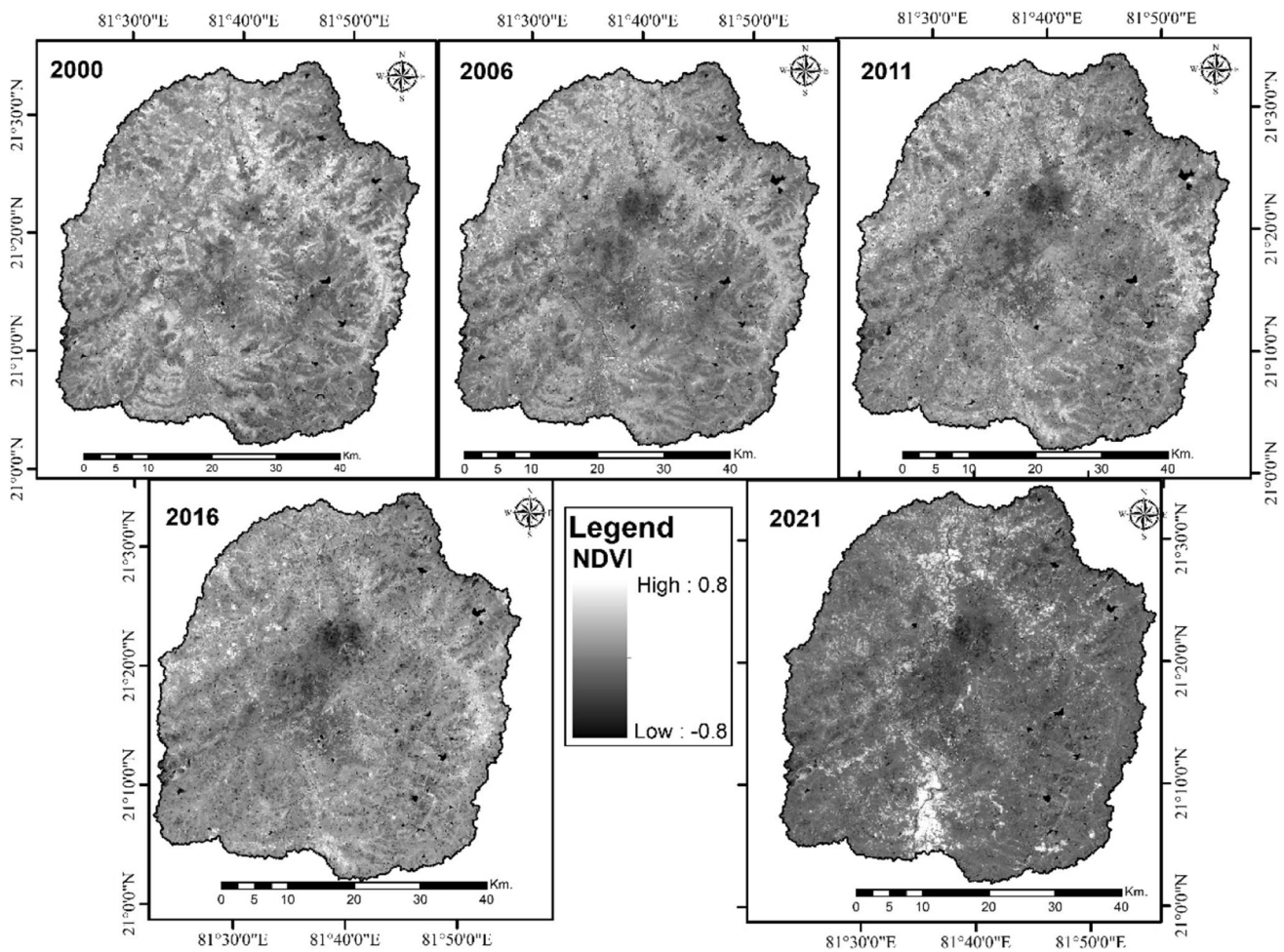


Fig. 4 NDVI from year 2000 to 2021

Table 2 Value for C<sub>0</sub>–C<sub>6</sub>SW coefficient constant

| S. No | Constant       | Value    |
|-------|----------------|----------|
| 1     | C <sub>0</sub> | -0.268   |
| 2     | C <sub>1</sub> | 1.378    |
| 3     | C <sub>2</sub> | 0.138    |
| 4     | C <sub>3</sub> | 54.300   |
| 5     | C <sub>4</sub> | -2.238   |
| 6     | C <sub>5</sub> | -129.200 |
| 7     | C <sub>6</sub> | 16.400   |

$$L\lambda = (L\lambda_{\max} - L\lambda_{\min} / QCal_{\max} - QCal_{\min}) * (QCal - QCal_{\min}) + L\lambda_{\min} \quad (1)$$

where  $L\lambda$  is the value of the cell as radiance,  $QCal$  is the digital number of each pixel,  $L\lambda_{\min}$  is the minimum spectral radiance scales to  $QCal_{\min}$  and  $L\lambda_{\max}$  is the maximum spectral radiance scales to  $QCal_{\max}$ , and  $QCal_{\min}$  and  $QCal_{\max}$  are the minimum and maximum quantized calibrated pixel

value (which typically lies between 0 and 255 respectively) or the second equation used for calculation radiance is:

$$L\lambda = ML * Qcal + AL \quad (2)$$

where  $L\lambda$  - top of atmospheric spectral radiance in watts/(m<sup>2</sup>\*srad\*μm),  $ML$  - band-specific multiplicative rescaling factor (radiance\_mult\_band taken from Meta data file),  $Qcal$  is the calibrated, quantized standard pixel values of digital number and  $AL$  is band-specific additive rescaling factor given in the meat data file.

### Calculating NDVI

NDVI is an index used to measure the overall green area in image; it can be therefore used to enhancing the area with vegetation cover. NDVI was calculated as the ratio between measured reflectance values of Red band and near infrared

**Table 3** Difference in LULC area from 2000 to 2021

| S. No             | Feature     | 2000            | 2006            | 2011            | 2016            | 2021            |
|-------------------|-------------|-----------------|-----------------|-----------------|-----------------|-----------------|
| 1                 | Cultivation | 1906.014        | 1976.563        | 1955.435        | 2051.616        | 2036.904        |
| 2                 | Open Land   | 270.545         | 329.782         | 349.197         | 174.614         | 164.710         |
| 3                 | Settlement  | 83.251          | 134.805         | 173.601         | 255.531         | 286.273         |
| 4                 | Vegetation  | 225.841         | 50.511          | 14.886          | 12.891          | 10.586          |
| 5                 | Waterbody   | 56.161          | 50.151          | 48.693          | 47.161          | 43.338          |
| <b>Total area</b> |             | <b>2541.812</b> | <b>2541.812</b> | <b>2541.812</b> | <b>2541.812</b> | <b>2541.812</b> |

(NIR) band of the images which is done using the following formula (Rouse et al. 1974).

$$\text{NDVI} = \frac{\text{NIR} - \text{Red}}{\text{NIR} + \text{Red}} \quad (3)$$

where NIR and Red mentioned in the formula are the near infrared and Red bands of the image.

NDVI values were computed for the current work to investigate its relationship with LST. It has been found that index value may vary from  $-1.0$  to  $1.0$ , with higher values associated with greater levels of healthy vegetation cover; this is because in the near infrared spectrum, green vegetation gives high reflectance than it does in the visible spectrum (Rajeshwari and Mani 2014; Sobrino et al. 2004; Sun and Kafatos 2007). Higher reflectance values for nir can be seen for clouds, water, and snow; correspondingly, lower reflectance values can be seen for rock surfaces and bare soil. The NDVI values for these features therefore ranged from  $+0.8$  to  $+0.65$ , with higher values indicating greater plant canopy density and greenness, while values for nearby bare soil and rocks are close to 0, and for other surface water bodies, negative index values are present (Tucker et al. 1986; Xiao and Weng 2007) (Fig. 4).

Once the spectral irradiance from Landsat TM data is extracted, thereafter, surface temperature can be calculated using the equation below:

$$T_B = K2 \ln(K1 L + 1) - 273.15 \quad (4)$$

where  $T_B$  represents the surface temperature values for Landsat 5, K1 and K2 are thermal conversion constants (value is given in the Metadata file). Constant values were in Kelvin, which were converted into Celcius ( $^{\circ}\text{C}$ ) by subtracting it with  $-273.15$  (Qin et al. 2004; Mukherjee et al. 2014). Proportion of land covered by vegetation is measured by  $\rho v$  (Avdan and Jovanovska 2016; Salih et al. 2018 and Jaiswal and Jhariya 2020). The classed NDVI image is applied to calculate the proportions of plant and bare soil.

$$\rho v = \left( \text{NDVI} - \text{NDVI}_s / \text{NDVI}_v - \text{NDVI}_s \right)^2 \quad (5)$$

Here,  $\text{NDVI}_s$  indicates the lowest NDVI value obtained through data file's metadata, showing the presence of bare soil, and  $\text{NDVI}_v$  represents the highest value, indicating a rich natural vegetation (Guha et al. 2018; Srivastava et al. 2010).

Emissivity can be defined as the capacity of the surface to absorb radiation (Alhawiti and Mitsova 2016). The kind of soil, the roughness of the surface, and the type of vegetation cover are all factors that affect LSE [23]. The subsequent equation with LSE was used to obtain:

$$\varepsilon = \varepsilon_{v\lambda} * \rho v + \varepsilon_{s\lambda} * (1 - \rho v + C_\lambda) \quad (6)$$

where  $\varepsilon$  is the land surface emissivity,  $\varepsilon_{s\lambda}$  and  $\varepsilon_{v\lambda}$  represent emissivity of soil and vegetation respectively,  $\rho v$  is the proportion of vegetation, and  $C_\lambda$  is equal to the surface roughness taken as a constant value of 0.009 (Salih et al. 2018; Abdalkadhum et al. 2020).

Soil is considered to be the type of land cover emissivity for which has been taken as 0.096. While values around 0.2 and 0.5 are taken into account as a mix of soil and vegetation cover, the emissivity is determined using the above equation (Mallick et al. 2012; Rajeshwari and Mani 2014). In the last instance, vegetation cover is considered when the Normalize Difference Vegetation Index value is larger than 0.5, for which the value taken was 0.97 (Rajeshwari and Mani 2014; Jeevalakshmi et al. 2016).

The final step for computation of LST was done using the equation (Weng et al. 2004; Kumar et al. 2017; Alhawiti and Mitsova 2016; Guha et al. 2018) for Landsat 7 ETM and

$$\text{LST} = \frac{T_B}{1 + \left( \lambda + \frac{T_B}{\rho} \right) * \ln \varepsilon} \quad (7)$$

where  $T_B$  is the temperature brightness,  $\lambda$  is the wavelength of the emitted radiance which is equal to  $11.5\mu\text{m}$ , and  $\varepsilon$  is the spectral emissivity and:

$$\rho = h.c / \sigma \quad (8)$$



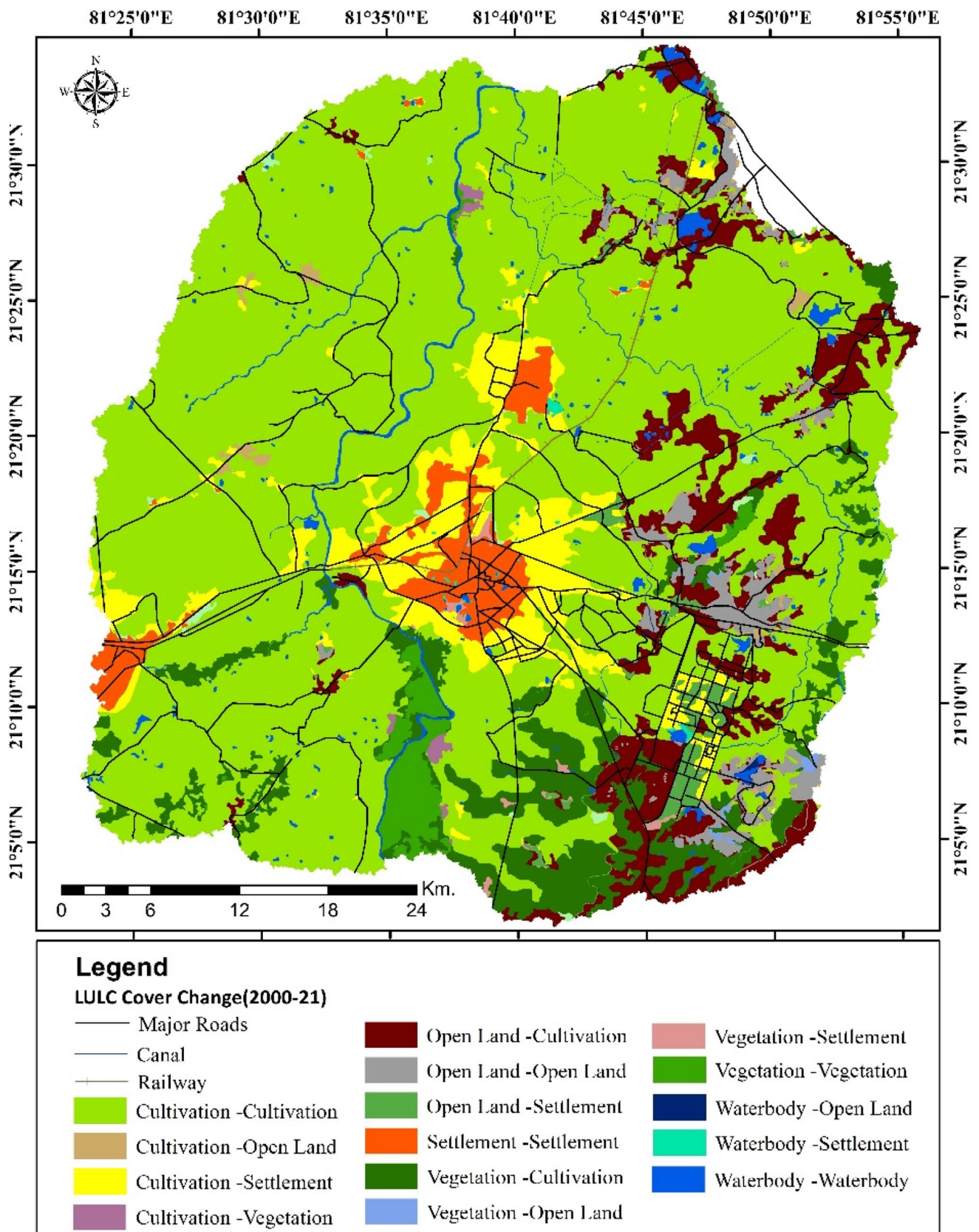


Fig. 5 Change in LULC

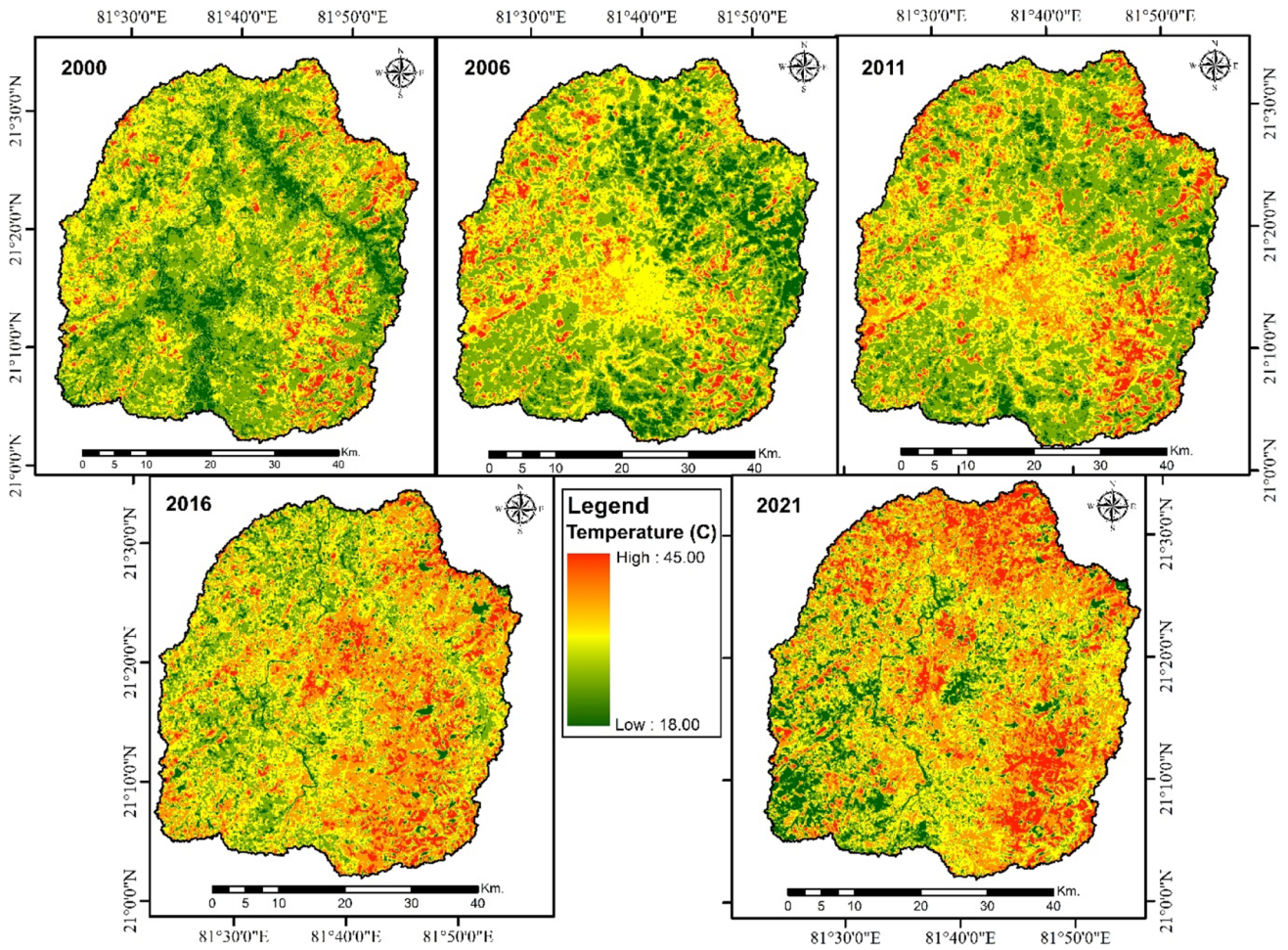
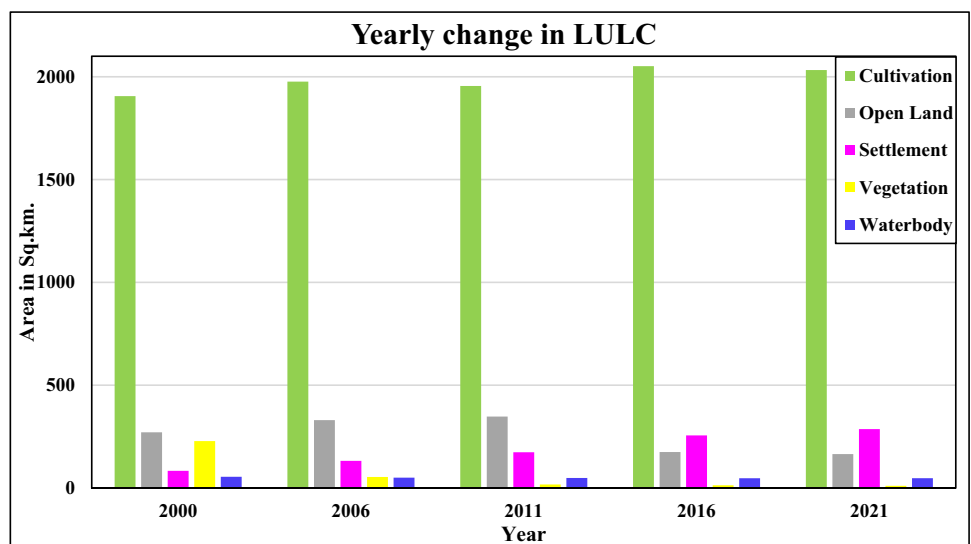


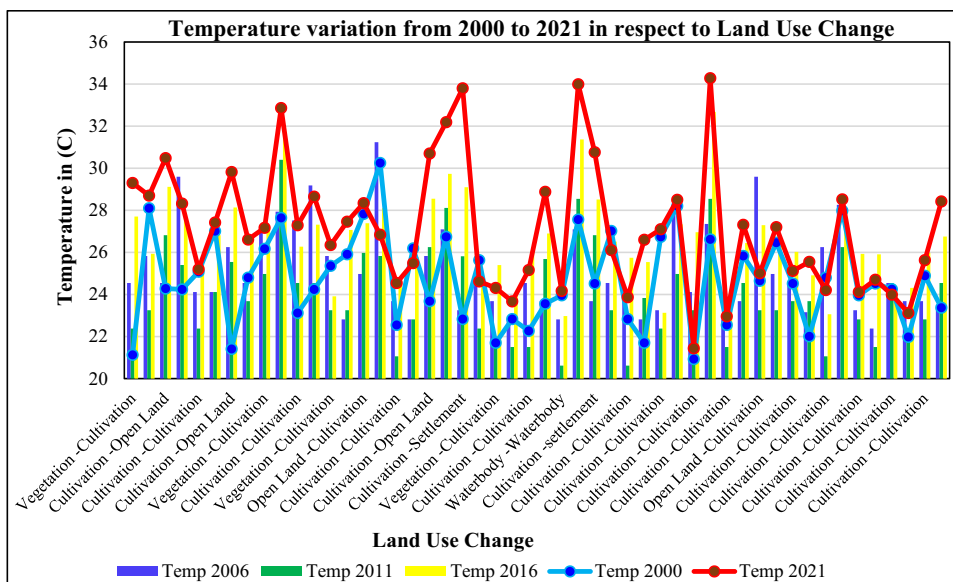
Fig. 6 Variation in LST with changing land use from 2000 to 2021

Fig. 7 Changes in LST from 2000 to 2021





**Fig. 8** Changes in LULC class from 2000 to 2021



Here,  $\sigma$  = Stefan Boltzmann’s constant is  $5.67 \times 10^{-8} \text{ W m}^{-2} \text{ K}^{-4}$ ,  $h$  = Plank’s constant ( $6.626 \times 10^{-34} \text{ J s}$ ),  $c$  = velocity of light ( $2.998 \times 10^8 \text{ m/s}$ ).

LST for Landsat 8 using the equation below:

$$LST = TB_{10} + C_1(TB_{10}-TB_{11}) + C_2(TB_{10}-TB_{11})^2 + C_0 + (C_3 + C_4W)(1-\epsilon) + (C_5 + C_6W)\Delta\epsilon \tag{9}$$

where LST is in Kelvin (K), C0 to C6 (given in Table 2) are the split-window (SW) coefficient range (Rajeshwari and Mani 2014; Kamran et al. 2015; Jaiswal and Jhariya 2020; Sobrino et al. 2004),  $TB_{10}$  and  $TB_{11}$  are the brightness temperatures of bands 10 and 11, and denotes the mean LSE derived value.

From TIR bands,  $W$  defines the atmospheric water vapor content and  $\Delta\epsilon$  defines the difference in surface temperature of two bands (B10 and B11)

**Calculation of NDBI**

NDBI is an automated index used to calculate the built-up area specifically in the city region. It always shows a strong to moderately strong positive correlation (Zha et al. 2003), no matter what time of year it is. It is a most important index which has its effect over LST . Also, the growth of built-up areas is common process of urbanization occurring all over the world; therefore, the importance of NDBI is slowly growing in LST-related studies (Guha et al. 2021). A long-term seasonal analysis on the relationship between LST and NDBI using Landsat data. Quaternary International, 575, 249-258.).

The NDBI is determined by taking the ratio of the values obtained from the shortwave infrared (SWIR) and the near

infrared (NIR) band of the Landsat imagery (Alademomi et al. 2022) for all the years.

$$NDBI = (SWIR-NIR)/(SWIR + NIR)$$

**Results**

The results obtained from the above study demonstrated a relatively higher variance in temperature at places with dense urbanization and with fewer waterbodies and vegetation cover (Fatemi and Narangifard 2019; Feizizadeh et al. 2013; Alhawiti and Mitsova 2016) while in the areas with higher vegetation shows lower surface temperature; this may be because of such thick vegetation cover, or clear waterbodies at those places. It has also been observed that since the last two decades (Table 3), a lot of urban sprawl has occurred, due to which there was a decrease in cultivation and vegetation area resulting in higher temperature values for such sites (Rajeshwari and Mani 2014).

**The LULC change analysis**

The primary LULC types in the research area were cultivation, open land, settlement, vegetation, and water bodies. Urbanized area grew overall from 83.251 km<sup>2</sup> in 2000 to 286.273 km<sup>2</sup> in 2021 with continuous increase during 2006, 2011, and 2016, an increase of around 8% over the course of the years. Natural landscapes like vegetation and water body regions constantly declined between 2000 and 2021.

**Table 4** Location of random points taken for LST comparison

| S. No | Land use change         | LST 2000 | LST 2006 | LST 2011 | LST 2016 | LST 2021 | Latitude | Longitude |
|-------|-------------------------|----------|----------|----------|----------|----------|----------|-----------|
| 1     | Settlement-Settlement   | 25.362   | 27.095   | 21.941   | 24.517   | 33.124   | 21.249   | 81.634    |
| 2     | Cultivation-Settlement  | 23.686   | 23.683   | 24.115   | 25.797   | 32.530   | 21.261   | 81.558    |
| 3     | Cultivation-Settlement  | 26.192   | 25.826   | 22.815   | 25.470   | 31.987   | 21.240   | 81.700    |
| 4     | Cultivation-Settlement  | 29.187   | 30.420   | 24.545   | 24.494   | 33.255   | 21.320   | 81.636    |
| 5     | Cultivation-Settlement  | 26.192   | 25.401   | 22.815   | 24.032   | 32.302   | 21.200   | 81.639    |
| 6     | Settlement-Settlement   | 21.128   | 22.815   | 18.833   | 20.245   | 27.765   | 21.362   | 81.671    |
| 7     | Cultivation-Settlement  | 27.016   | 26.674   | 24.973   | 26.138   | 34.207   | 21.387   | 81.647    |
| 8     | Settlement-Settlement   | 27.289   | 28.352   | 25.401   | 27.045   | 34.460   | 21.386   | 81.681    |
| 9     | Cultivation-Settlement  | 30.259   | 28.352   | 25.826   | 25.528   | 35.503   | 21.357   | 81.646    |
| 10    | Cultivation-Settlement  | 29.724   | 27.095   | 25.401   | 26.794   | 35.132   | 21.329   | 81.631    |
| 11    | Settlement-Settlement   | 27.016   | 25.826   | 23.683   | 25.612   | 34.682   | 21.183   | 81.410    |
| 12    | Cultivation-Settlement  | 29.992   | 31.238   | 25.826   | 27.371   | 35.480   | 21.273   | 81.528    |
| 13    | Cultivation-Settlement  | 29.456   | 27.934   | 24.115   | 25.089   | 33.767   | 21.250   | 81.519    |
| 14    | Cultivation-Cultivation | 33.162   | 29.597   | 24.545   | 24.379   | 36.160   | 21.361   | 81.502    |
| 15    | Cultivation-Open Land   | 31.057   | 27.934   | 25.826   | 27.661   | 36.610   | 21.322   | 81.488    |
| 16    | Waterbody-Waterbody     | 29.992   | 21.502   | 17.930   | 20.881   | 27.270   | 21.241   | 81.744    |
| 17    | Cultivation-Settlement  | 29.456   | 27.934   | 24.115   | 27.072   | 34.570   | 21.179   | 81.778    |
| 18    | Open Land-Settlement    | 31.322   | 30.420   | 25.401   | 27.959   | 34.541   | 21.157   | 81.799    |
| 19    | Cultivation-Cultivation | 31.322   | 31.645   | 26.251   | 28.049   | 35.894   | 21.197   | 81.879    |
| 20    | Open Land-Open Land     | 32.639   | 33.262   | 27.516   | 28.022   | 32.807   | 21.213   | 81.819    |
| 21    | Open Land-Open Land     | 33.162   | 32.051   | 27.516   | 27.973   | 35.940   | 21.235   | 81.822    |
| 22    | Cultivation-Cultivation | 28.648   | 22.815   | 24.115   | 29.266   | 34.421   | 21.261   | 81.777    |
| 23    | Open Land-Cultivation   | 31.586   | 29.597   | 25.826   | 28.076   | 35.658   | 21.271   | 81.839    |
| 24    | Open Land-Settlement    | 29.187   | 27.516   | 25.401   | 27.948   | 33.974   | 21.110   | 81.778    |
| 25    | Open Land-Settlement    | 29.724   | 28.352   | 26.251   | 25.334   | 32.556   | 21.136   | 81.784    |
| 26    | Cultivation-Settlement  | 26.742   | 27.095   | 23.683   | 26.585   | 34.251   | 21.157   | 81.772    |
| 27    | Waterbody-Waterbody     | 27.289   | 22.379   | 18.382   | 20.620   | 26.621   | 21.147   | 81.770    |
| 28    | Vegetation-Cultivation  | 25.084   | 24.973   | 21.502   | 24.477   | 31.942   | 21.192   | 81.611    |
| 29    | Cultivation-Cultivation | 26.192   | 25.401   | 21.941   | 27.152   | 33.081   | 21.125   | 81.574    |
| 30    | Vegetation-Vegetation   | 30.259   | 28.768   | 24.545   | 22.700   | 30.729   | 21.159   | 81.604    |
| 31    | Open Land-Settlement    | 27.289   | 26.674   | 22.379   | 25.331   | 32.929   | 21.069   | 81.680    |
| 32    | Vegetation-Cultivation  | 30.525   | 25.826   | 23.250   | 26.489   | 34.544   | 21.114   | 81.501    |
| 33    | Cultivation-Cultivation | 28.377   | 24.545   | 24.545   | 25.811   | 35.451   | 21.120   | 81.406    |
| 34    | Cultivation-Settlement  | 28.918   | 26.251   | 22.815   | 25.975   | 35.137   | 21.232   | 81.409    |
| 35    | Cultivation-Cultivation | 31.322   | 29.597   | 25.826   | 27.951   | 34.583   | 21.376   | 81.552    |
| 36    | Cultivation-Cultivation | 31.057   | 30.009   | 26.251   | 27.981   | 36.705   | 21.417   | 81.508    |
| 37    | Cultivation-Cultivation | 26.742   | 24.115   | 22.815   | 25.506   | 33.759   | 21.465   | 81.559    |
| 38    | Cultivation-Cultivation | 26.192   | 23.683   | 21.502   | 26.456   | 30.839   | 21.517   | 81.742    |
| 39    | Cultivation-Cultivation | 27.289   | 25.401   | 22.379   | 24.340   | 31.836   | 21.504   | 81.790    |
| 40    | Open Land-Open Land     | 32.639   | 32.456   | 26.674   | 29.093   | 35.565   | 21.500   | 81.809    |
| 41    | Cultivation-Open Land   | 28.377   | 29.183   | 25.826   | 26.984   | 35.591   | 21.523   | 81.805    |
| 42    | Cultivation-Cultivation | 28.918   | 26.251   | 24.115   | 26.781   | 33.725   | 21.567   | 81.756    |
| 43    | Cultivation-Cultivation | 29.456   | 30.009   | 25.401   | 26.761   | 34.791   | 21.383   | 81.726    |
| 44    | Open Land-Open Land     | 31.057   | 28.768   | 27.934   | 29.206   | 36.188   | 21.343   | 81.851    |
| 45    | Open Land-Cultivation   | 31.850   | 31.645   | 27.095   | 28.670   | 36.577   | 21.288   | 81.790    |
| 46    | Cultivation-Cultivation | 30.259   | 24.973   | 22.815   | 25.919   | 33.494   | 21.270   | 81.910    |



**Table 5** Statistical data of NDBI

| S. No           | 2000    | 2006    | 2011    | 2016    | 2021    |
|-----------------|---------|---------|---------|---------|---------|
| <b>Min.</b>     | -0.3526 | -0.3623 | -0.4333 | -0.4237 | -0.5188 |
| <b>Max.</b>     | 0.3895  | 0.3752  | 0.3522  | 0.3669  | 0.3960  |
| <b>Mean</b>     | 0.1315  | 0.0841  | 0.0574  | 0.0638  | 0.0203  |
| <b>St. Dev.</b> | 0.1403  | 0.1356  | 0.1345  | 0.1330  | 0.1918  |

**Table 6** Statistical data of NDVI

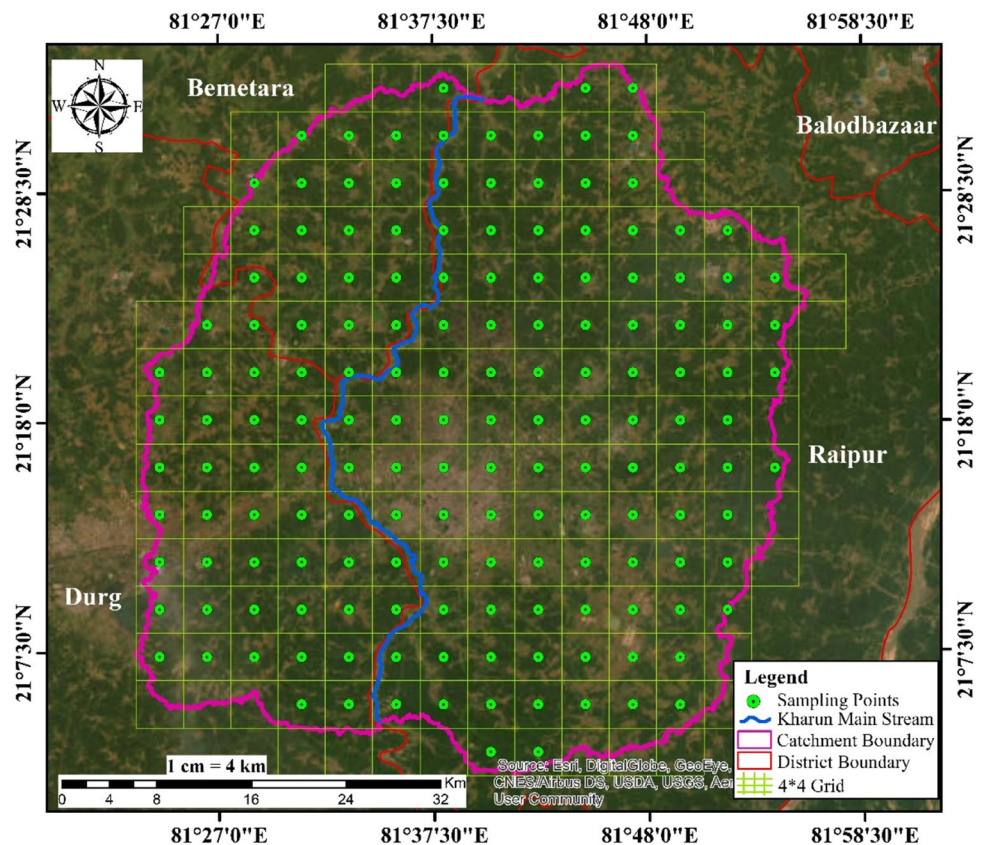
| S. No           | 2000    | 2006    | 2011    | 2016    | 2021    |
|-----------------|---------|---------|---------|---------|---------|
| <b>Min.</b>     | -0.4800 | -0.1702 | -0.2163 | -0.2035 | -0.1219 |
| <b>Max.</b>     | 0.5968  | 0.4888  | 0.4909  | 0.4405  | 0.6866  |
| <b>Mean</b>     | 0.2592  | 0.2356  | 0.2244  | 0.2200  | 0.2354  |
| <b>St. Dev.</b> | 0.1437  | 0.0949  | 0.1008  | 0.0822  | 0.1205  |

While there was less variance in the water body area, the vegetation area shrunk from 227.840 to 10.586 km<sup>2</sup>, possibly as a result of the establishment of numerous artificial ponds around the study region to fulfil the scarcity. Along with the urban area cultivation area expanded as well from 2000 to 2021, which was 1906.014, 1976.563, 1955.435, 2051.616,

and 2032.904 km<sup>2</sup> for each of the included years. In 2000, this area was covered by vegetation; now, it is open land or settlement area. Table 3 provides specific changes in the area and during the year.

The main city area of Raipur is situated in the center of the study region, where the analysis findings indicate that the significant LULC developments have occurred. More urban expansion seemed to occur from 2011 in the study area’s southeast and southwest region where Naya Raipur and part of Durg city area comes. The change analysis thus relates to those regions where land has changed between 2000 and 2021 (Basha et al. 2018) which is shown in Fig. 5. Due to this, major changes can be seen in the maps created for 2006 and 2011. The research area’s green vegetation has been observed to be declining over the years, particularly in the vicinity of major metropolitan areas. The idea is that the LULC change (Fig. 6) is connected to the changes in the NDVI and is connected to LST (Gogoi et al. 2019) which was also calculated for same years (Fig. 7). Classified maps for LULC show continuous variation in area during 2000 to 2021, which are shown in Fig. 8. For the accuracy of classified LULC map, the data has been cross checked with Google images with the help of 46 random sample with equal points for each specific class (see Table 4). Results show between 90 and 95% of the classified LULC maps (Nayak and Mandal 2019).

**Fig. 9** Grid wise presentation of sampling points in study area



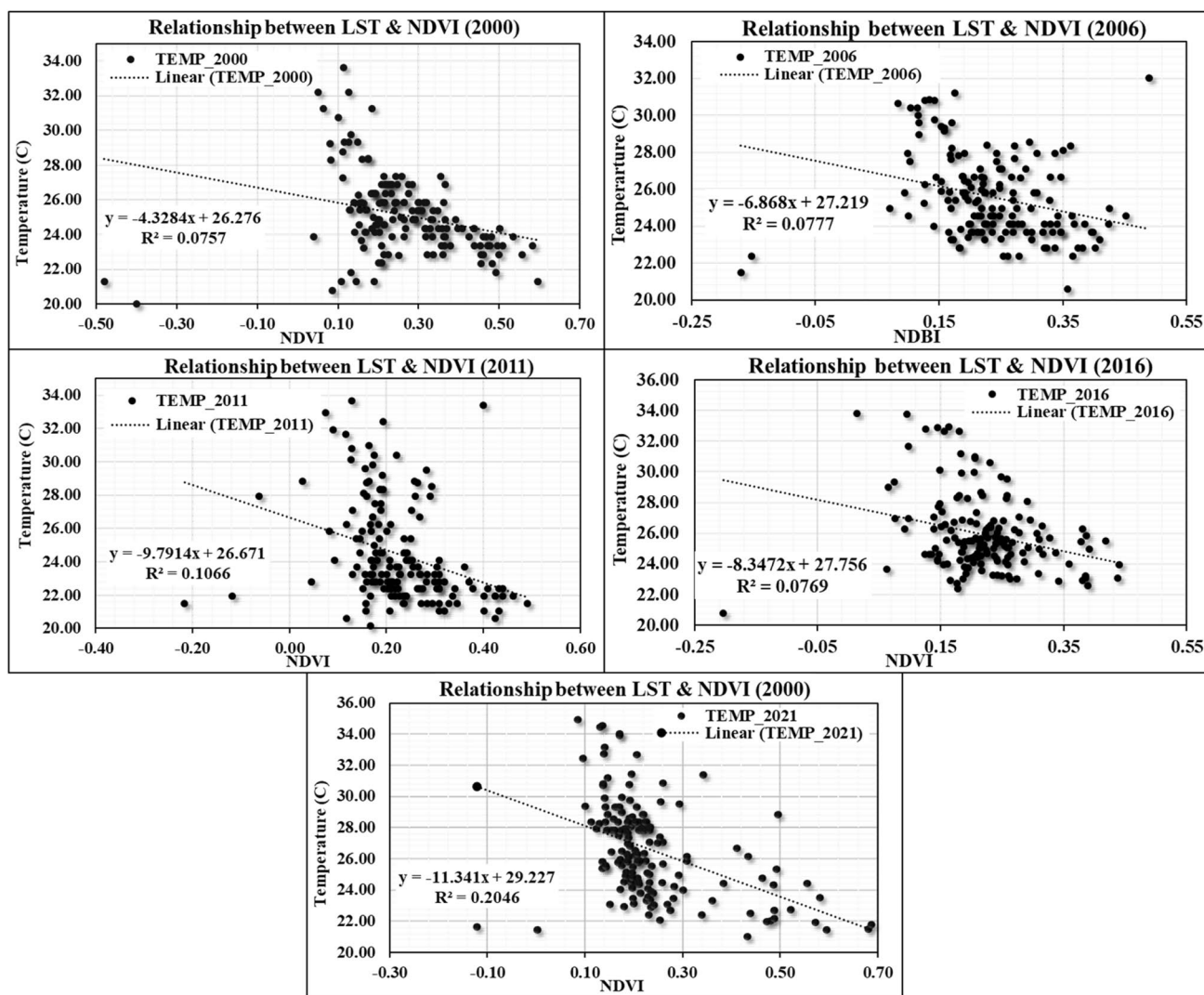


**Fig. 10** Scatterplot showing correlation of LST with NDVI for years 2000, 2006, 2011, 2016 and 2021(a to e)

### Interrelationship between changing LST and urbanization

In the previous sections, we found that the surface temperature increased due to change in surface condition of land during the period 2000 to 2021 (Feizizadeh et al. 2013). Maximum changes occurred in the central part of basin with main city area of Raipur district and in the small part of eastern basin constituting the Naya Raipur region during 2011 to 2021. The pattern of LULC, NDVI, and LST represents the same trends; also by the LST values represented by the random points, it has been observed that the transformed areas with settlement have relatively high LST which shows a clear relationship between all the three parameters and LULC change is directly associated with the global

warming. For example, city regions of Raipur and Durg which are highly populated cities of Chhattisgarh experience relatively higher rate of increasing temperature during the years 2000 to 2021 than that nearby towns or villages distributed in small patches throughout the study area. Forty-six random points showing the variation in LULC class with respect to variation in the temperature shown in Fig. 6 clearly signify that changing LULC has its clear impact on to the rising surface temperature.

### Relationship between NDBI, NDVI, and LST

NDBI values calculated for the study area shows that the values were more at the places dense urbanization (Chen et al. 2013) including the city area of Raipur city, Naya Raipur

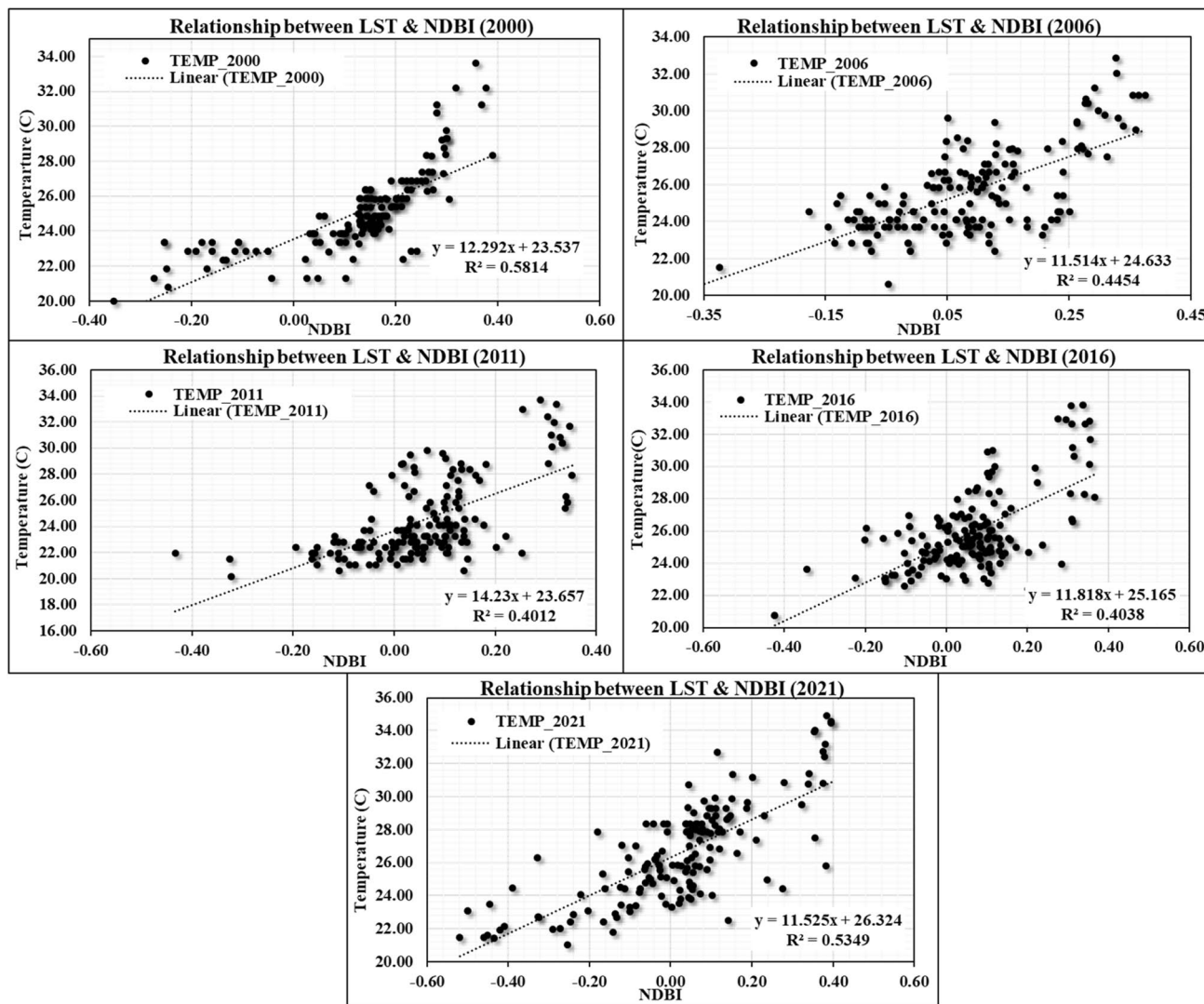


Fig. 11 Scatterplot showing correlation of LST with NDBI for years 2000, 2006, 2011, 2016, and 2021(a to e)

and very small part of Bhilai, Durg District located at the southeastern and southwest corner of the study area respectively while the NDVI value is higher with the area covered with vegetation coming under the study area. Since the area has huge variation in type of land use, therefore NDBI and NDVI varied between  $-0.519$  to  $0.396$  and  $-0.480$  to  $0.596$  respectively. Tables 5 and 6 show NDVI and NDBI values all the years from 2000 to 2021 for the considered years. To determine the relationship between NDBI, NDVI, and LST, overall 159 points were taken which were equally distributed throughout the study area; these points were the center point of each grid of  $4 \times 4$  km (shown in Fig. 9). In order to find the correlation among all the three parameters, linear regression method was used (Chen et al. 2013; Gorgani et al.

2013). It has been observed that there was positive relationship between NDBI and LST with  $R^2$  value ranging between 0.4 and 0.58. As with the increasing values of NDBI, values were increasing and vice versa while in the case of NDVI, correlation seems to be negative as the increasing values of NDVI (ranging between 0.07 and 0.1) denote the vegetation cover which represents lower LST values (Sun and Kafatos 2007). Relationship of LST with NDVI and NDBI is represented in Figs. 10 and 11.

$$R^2 = \frac{SSR}{SST} = \frac{\sum (\hat{y}_i - \bar{y})^2}{\sum (y_i - \bar{y})^2} \tag{10}$$



**Fig. 12** Statistical representation of LST range from 2000 to 2021

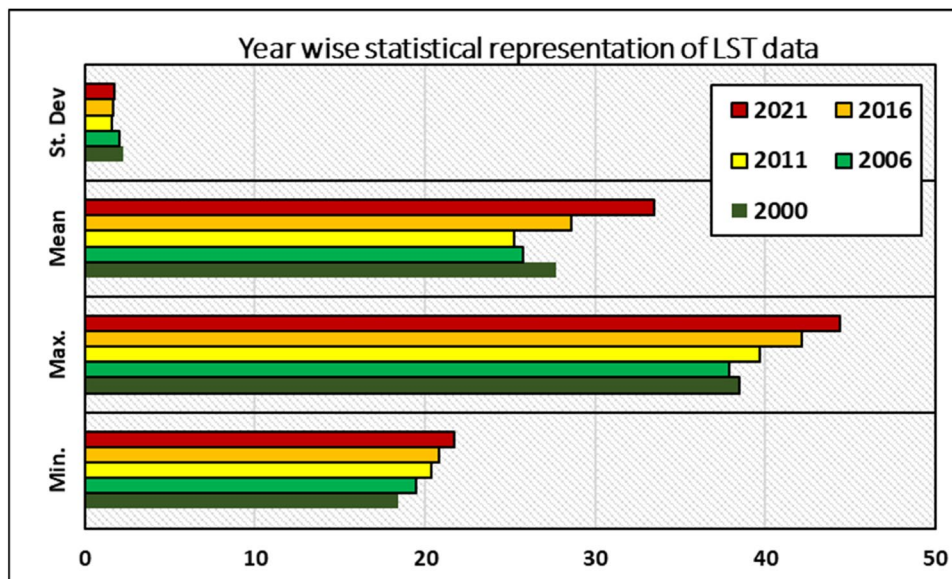


**Table 7** Statistical data of LST

| Year           | 2000   | 2006   | 2011   | 2016   | 2021   |
|----------------|--------|--------|--------|--------|--------|
| <b>Min.</b>    | 18.392 | 19.49  | 20.342 | 20.821 | 21.728 |
| <b>Max.</b>    | 38.462 | 37.867 | 39.663 | 42.128 | 44.445 |
| <b>Mean</b>    | 27.736 | 25.785 | 25.22  | 28.606 | 33.479 |
| <b>St. Dev</b> | 2.239  | 2.021  | 1.543  | 1.632  | 1.746  |

where SSR and SST are sum of squares of residuals and total sum of squares respectively,  $R^2$  represents coefficient of determination,  $\hat{y}$ ,  $\bar{y}$ , and  $y_i$  represent the prediction or a point on the regression line, mean of all the values, and the actual values respectively.

### Changes in LST

Variation in surface temperature has been represented in a graphical representation for all the 5 years for the area of interest shown in Fig. 6 which shows Urban Heat Island (UHI) effect which means higher temperature values were much more concentrated in the city areas (Fig. 6). An overall increase of about  $5.65^\circ\text{C}$  is observed since the last two decades in the study area. Also there was noticeable variation in temperature with changing land use. Highest temperature values were recorded in the middle of cities and at outer stretch of the city region where the industrial growth appeared temperature rose more during 2011–2021 at newly

formed area like Naya Raipur region which has very less waterbodies or vegetation. Statistical calculation was done for all the years to see the variation in the temperature and the difference in the minimum, maximum, and mean temperature values is given in Fig. 12 and Table.7 which shows that with changing land use, LST is changing, increasing urbanization resulted in increasing surface temperature for the transformed area.

### Cross-validation of Landsat retrieved LST

MOD11A1 LST data is a daily L3 (level3) that gives daily land surface temperature and emissivity data. It has been gridded using the sinusoidal projection with a spatial resolution of about 1 km where the actual grid size is 0.928 km by 0.928 km. One tile of a product is divided into 1200 rows and columns (Wan 2007; Srivastava et al. 2009). This satellite-derived data has been used to validate the Landsat retrieved LST data; this validation technique of cross-validation has been used by different researchers in the past till date (Chan and Chung-Pai 2018; Nikam et al. 2016) as there were no LST data from the ground that could be used in this study (Aik et al. 2020; Mukherjee et al. 2014). The MODIS LST has been projected from sinusoidal to the UTM projection system and further subset was created for all the 5 years to create a subset of MODIS LST for the study area. From the point of view of validation, 159 sites were selected by dividing the area into grid (Fig. 9) with an area of  $16\text{km}^2$  each and considering its center point for sample. As the resolution for both the satellites differs from



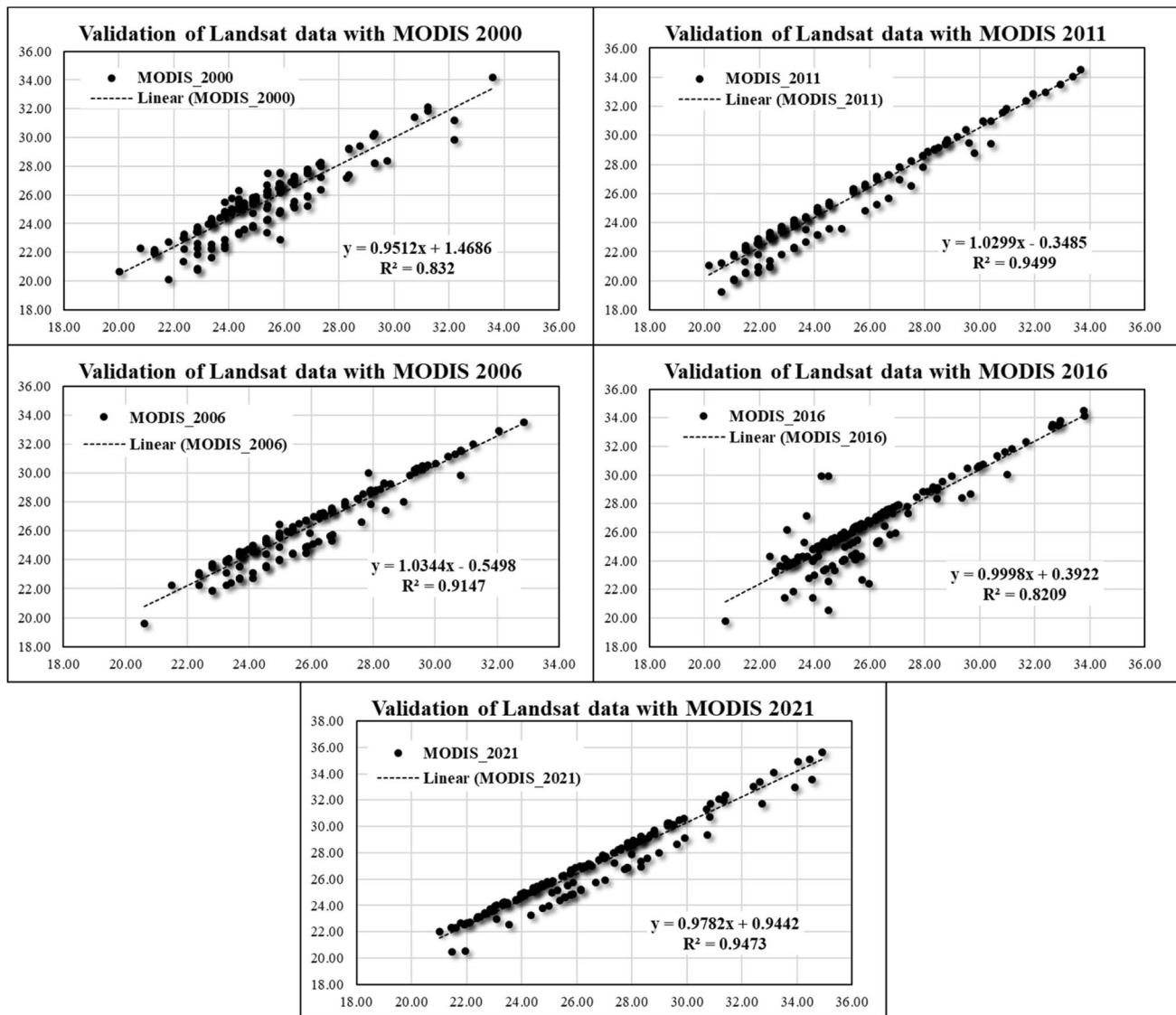


**Fig. 13** Scatterplot showing comparison of Landsat-derived LST with MODIS-derived LST for years 2000, 2006, 2011, 2016, and 2021(a to e)

each other, therefore Landsat data has been resampled using the interpolation technique (Nikam et al. 2016; Yang and Huang 2014). Zonal statistical method in Qgis software is a type of statistical method which performs calculations on multiple pixel values belonging to a raster layer by using a polygonal vector layer. This method was performed by calculating the mean LST pixel values of all Landsat dataset for each sample coming inside the MODIS pixels selected (Vlassova et al. 2014). Cross-validation of retrieved mean LST values with same spatial reference was used for the validation step with MODIS-derived LST values and it was found that there was approx. average difference of  $\pm 1-2^{\circ}\text{C}$  at most of the places while at few places, the difference was

more which may be due to the difference in scale of the two datasets. The best visual representation method for contrasting two quantitative variables is a scatterplot with linear regression where  $r^2$  indicates a model's fit. The  $r^2$  coefficient of determination measures how closely regression predictions match real data points. The value of  $r^2$  from 0.7 and above considered to be a good data match. This method is used by different researchers for comparing and correlation of their data (Bosilovich 2006 and Duan et al. 2017) for the comparison of temperature values derived from Landsat data with MODIS-derived data. Obtained results show the high value of  $r^2$  ranging between 0.82 and 0.94 (Fig. 13).

## Discussion and conclusion

Rapid urbanization due to the changing land use has shown an increasing effect on surface temperature which is a common phenomenon all across the world. These changes in LULC depend on many factors including the extent, elevation, and physiography. It can be considered that the rate of increase LST is more in most of the developing cities across India. In reference to the study area which is has shown huge development in the central and southern part during 2011 to 2016 and still is in developing phase, it has been observed that there is overall variation of  $\sim 5.74$  °C in mean LST from 2000 to 2021. This decadal increase in temperature induced as effect of changing LULC requires urgent attention and investigations at local as well as regional level specifically for such areas where rapid and unplanned urbanization is taking place.

This study has been done with use thermal datasets with its processing under GIS platform for analysis and identification of variation in different parameters like LULC, LST, NDVI, and NDBI. It was observed that in the case of LKC, NDVI showed a strong negative correlation with LST while NDBI has shown its positive correlation with LST although the calculated  $R^2$  values were quite less which may be due to the large vegetation cover over the area as well but it can be clearly observed that built-up index is directly related to increasing LST.

Thus, the performed study illustrates that the GIS and remote sensing studies have excellent capabilities for conducting such studies; these techniques can be applied to derive an output with much ease and relatively faster, but due to lag in the dataset, the limited resolution of freely available datasets and sensor-generated distortions they lack in accuracy and detailed study. The above research can be furthermore extended by studying influencing parameters in detail. Also, accuracy assessment can be done using other available datasets and ground truth verification.

**Data availability** The data that support the findings of this study are openly and freely available. (Details of used data are mentioned in a table along with the source within the manuscript in “List of Table” section).

**Author contribution** All authors contributed to the study. Material preparation, data collection and analysis, and first drafting were performed by Mrs. Tanushri Jaiswal. The conceptualization, review, and editing were done by all authors (Mrs. Tanushri Jaiswal, Dr. Dalchand Jhariya, and Dr. Surjeet Singh). All authors read and approved the final manuscript.

## Declarations

**Ethical approval** Not applicable.

**Consent to participate** Not applicable.

**Consent for publication** Not applicable.

**Conflict of interest** The authors declare no competing interests.

## References

- Abdalkadhum AJ, Salih MM, Jasim OZ (2020) Combination of visible and thermal remotely sensed data for enhancement of Land Cover Classification by using satellite imagery. In: IOP Conference Series: Materials Science and Engineering (Vol. 737, No. 1, p. 012226). IOP Publishing
- Adegoke JO, Pielke RA Sr, Eastman J, Mahmood R, Hubbard KG (2003) Impact of irrigation on midsummer surface fluxes and temperature under dry synoptic conditions: a regional atmospheric model study of the US High Plains. *Mon Weather Rev* 131:556–564
- Aik J, Chua R, Jamali N, Chee E (2020) The burden of acute conjunctivitis attributable to ambient particulate matter pollution in Singapore and its exacerbation during South-East Asian haze episodes. *Sci Total Environ* 740:140129
- Alademomi AS, Okolie CJ, Daramola OE, Akinnusi SA, Adediran E, Olanrewaju HO et al (2022) The interrelationship between LST, NDVI, NDBI, and land cover change in a section of Lagos metropolis. *Nigeria Applied Geomatics* 14(2):299–314
- Alhawiti RH, Mitsova D (2016) Using Landsat-8 data to explore the correlation between Urban Heat Island and Urban Land uses. *IJRET: International Journal of Research. Eng Technol* 5(3):457–466
- Anderson JR (1976) A land use and land cover classification system for use with remote sensor data (Vol. 964). US Government Printing Office
- Avdan U, Jovanovska G (2016) Algorithm for automated mapping of land surface temperature using LANDSAT 8 satellite data. *Journal of Sensors* pp 1–8
- Babalola SO, Musa AA, Adegboyega SA, Abubakar T, Ezeomede IC (2014) Analysis of land use/land cover of Girei, Yola North and South Local Government Areas of Adamawa State, Nigeria using satellite imagery. *FUTY Journal of the Environment* 8(1):65–79
- Basha UI, Suresh U, Raju GS, Rajasekhar M, Veeraswamy G, Balaji E (2018) Landuse and landcover analysis using remote sensing and GIS: a case study in Somavathi River. Anantapur District, Andhra Pradesh, India *Nature Environment and Pollution Technology* 17(3):1029–1033
- Bosilovich MG (2006) A comparison of MODIS land surface temperature with in situ observations. *Geophys Res Lett* 33(20)
- Butt A, Shabbir R, Ahmad SS, Aziz N (2015) Land use change mapping and analysis using remote sensing and GIS: a case study of Simly watershed, Islamabad, Pakistan. *Egypt J Remote Sens Space Sci* 18:251–259
- Chan HP, Chung-Pai C (2018) Exploring and monitoring geothermal and volcanic activity using Satellite Thermal Infrared data in TVG, Taiwan. *TAO: Terrestrial, Atmospheric and Oceanic Sciences* 29(4):3
- Chaudhuri G, Mishra NB (2016) Spatio-temporal dynamics of land cover and land surface temperature in Ganges-Brahmaputra delta: a comparative analysis between India and Bangladesh. *Appl Geogr* 68:68–83
- Chen X, Zhao H, Li P, Yin Z (2006) Remote sensing image-based analysis of the relationship between urban heat island and land use/cover changes. *Remote Sens Environ* 104:133–146
- Chen L, Li M, Huang F, Xu S (2013) Relationships of LST to NDBI and NDVI in Wuhan City based on Landsat ETM+ image. In: 2013 6th International Congress on Image and Signal Processing (CISP) (Vol. 2, pp. 840–845). IEEE

- Ding H, Shi W (2013) Land-use/land-cover change and its influence on surface temperature: a case study in Beijing City. *Int J Remote Sens* 34(15):5503–5517
- Duan SB, Li ZL, Cheng J, Leng P (2017) Cross-satellite comparison of operational land surface temperature products derived from MODIS and ASTER data over bare soil surfaces. *ISPRS J Photogramm Remote Sens* 126:1–10
- Faqe Ibrahim GR (2017) Urban land use land cover changes and their effect on land surface temperature: case study using Dohuk City in the Kurdistan Region of Iraq. *Climate* 5(1):13
- Farid N, Moazzam MFU, Ahmad SR, Coluzzi R, Lanfredi M (2022) Monitoring the impact of rapid urbanization on land surface temperature and assessment of surface urban heat island using Landsat in megacity (Lahore) of Pakistan. *Front Remote Sens* 3:897397. <https://doi.org/10.3389/frsen>
- Fatemi M, Narangifard M (2019) Monitoring LULC changes and its impact on the LST and NDVI in District 1 of Shiraz City. *Arab J Geosci* 12:1–12
- Feizizadeh B, Blaschke T, Nazmfar H, Akbari E, Kohbanani HR (2013) Monitoring land surface temperature relationship to land use/land cover from satellite imagery in Maraqeh County. *Iran Journal of Environmental Planning and Management* 56(9):1290–1315
- Fonseka HPU, Zhang H, Sun Y, Su H, Lin H, Lin Y (2019) Urbanization and its impacts on land surface temperature in Colombo metropolitan area, Sri Lanka, from 1988 to 2016. *Remote Sens* 11(8):957
- Fu P, Weng Q (2016) A time series analysis of urbanization induced land use and land cover change and its impact on land surface temperature with Landsat imagery. *Remote Sens Environ* 175:205–214
- Gogoi PP, Vinoy V, Swain D, Roberts G, Dash J, Tripathy S (2019) Land use and land cover change effect on surface temperature over Eastern India. *Sci Rep* 9(1):1–10
- Gohain KJ, Mohammad P, Goswami A (2021) Assessing the impact of land use land cover changes on land surface temperature over Pune city, India. *Quat Int* 575:259–269
- Gorgani SA, Panahi M, Rezaie F (2013) The relationship between NDVI and LST in the urban area of Mashhad, Iran. In: *International Conference on Civil Engineering Architecture & Urban Sustainable Development 27&28 November* (p. 51)
- Guha S, Govil H, Dey A, Gill N (2018) Analytical study of land surface temperature with NDVI and NDBI using Landsat 8 OLI and TIRS data in Florence and Naples city, Italy. *European Journal of Remote Sensing* 51(1):667–678
- Guha S, Govil H, Gill N, Dey A (2021) A long-term seasonal analysis on the relationship between LST and NDBI using Landsat data. *Quat Int* 575:249–258
- Gupta R, Sharma LK (2020) Efficacy of Spatial Land Change Modeler as a forecasting indicator for anthropogenic change dynamics over five decades: A case study of Shoolpaneshwar Wildlife Sanctuary, Gujarat, India. *Ecol Indic* 112:106171
- Hamdi R (2010) Estimating urban heat island effects on the temperature series of Uccle (Brussels, Belgium) using remote sensing data and a land surface scheme. *Remote Sens* 2:2773–2784
- Herold M, Goldstein NC, Clarke KC (2003) The spatiotemporal form of urban growth: measurement, analysis and modeling. *Remote Sens Environ* 86:286–302
- How JinAik D, Ismail MH, Muharam FM (2020) Land use/land cover changes and the relationship with land surface temperature using Landsat and MODIS imageries in Cameron Highlands. *Malaysia Land* 9(10):372
- Idowu T E, Kiplangat N C and Waswa R (2019) Land cover changes and its implications on Urban Heat Island in Nairobi County: a GIS and remote sensing approach.
- Jaber HS, Shareef MA, Merzah ZF (2022) Object-based approaches for land use-land cover classification using high resolution quick bird satellite imagery (a case study: Kerbela, Iraq). *Geodesy and Cartography* 48(2):85
- Jaiswal T, Jhariya DC (2020) Impacts of land use land cover change on surface temperature and groundwater fluctuation in raipur district. *J Geol Soc India* 95(4):393–402
- Jeevalakshmi D, Reddy SN, Manikiam B (2016) Land cover classification based on NDVI using LANDSAT8 time series: a case study Tirupati region. In: *2016 International Conference on Communication and Signal Processing (ICCSP)*. IEEE, pp 1332–1335
- Jiang J, Tian G (2010) Analysis of the impact of land use/land cover change on land surface temperature with remote sensing. *Procedia Environ Sci* 2:571–575
- Joshi JP, Bhatt B (2012) Estimating temporal land surface temperature using remote sensing: a study of Vadodara urban area, Gujarat. *International Journal of Geology, Earth and Environmental Sciences* 2(1):123–130
- Kafi KM, Shafri HZM, Shariff ABM (2014) An analysis of LULC change detection using remotely sensed data: A Case study of Bauchi City. In *IOP conference series: Earth and Environmental Science* 20(1):012056
- Kamran KV, Pirnazar M, Bansouleh VF (2015) Land surface temperature retrieval from Landsat 8 TIRS: comparison between split window algorithm and SEBAL method. In *Third international conference on remote sensing and geoinformation of the environment (RSCy2015)* 9535:11–22
- Karakus CB (2019) The impact of land use/land cover (LULC) changes on land surface temperature in Sivas City Center and its surroundings and assessment of Urban Heat Island. *Asia-Pac J Atmos Sci* 55(4):669–684
- Kayet N, Pathak K, Chakrabarty A, Sahoo S (2016) Spatial impact of land use/land cover change on surface temperature distribution in Saranda Forest Jharkhand. *Modeling Earth Systems and Environment* 2(3):127
- Kumar N, Tischbein B, Kusche J, Laux P, Beg MK, Bogardi JJ (2017) Impact of climate change on water resources of upper Kharun catchment in Chhattisgarh, India. *Journal of Hydrology: Regional Studies* 13:189–207
- Lo CP, Quattrochi DA (2003) Land-use and land-cover change, urban heat island phenomenon, and health implications. *Photogramm Eng Remote Sens* 69(9):1053–1063
- Mallick J, Singh CK, Shashtri S, Rahman A, Mukherjee S (2012) Land surface emissivity retrieval based on moisture index from LANDSAT TM satellite data over heterogeneous surfaces of Delhi city. *Int J Appl Earth Obs Geoinf* 19:348–358
- McGrane SJ (2016) Impacts of urbanisation on hydrological and water quality dynamics and urban water management: a review. *Hydrol Sci J* 61(13):2295–2311
- Mohammad P, Goswami A (2019) Temperature and precipitation trend over 139 major Indian cities: an assessment over a century. *Modeling Earth Systems and Environment* 5(4):1481–1493
- Moss ML, Neill HO (2012) *Urban Mobility in the 21 st Century* NYU Rudin Center for Transportation Policy. Newyork
- Mukherjee S, Joshi PK, Garg RD (2014) A comparison of different regression models for downscaling Landsat and MODIS land surface temperature images over heterogeneous landscape. *Adv Space Res* 54(4):655–669
- Nayak S, Mandal M (2019) Impact of land use and land cover changes on temperature trends over India. *Land Use Policy* 89:104238
- Nikam BR, Ibragimov F, Chouksey A, Garg V, Aggarwal SP (2016) Retrieval of land surface temperature from Landsat 8 TIRS for

- the command area of Mula irrigation project. *Environ Earth Sci* 75(16):1–17
- Qin Z, Xu B, Zhang W, Li W, Chen Z (2004) Comparison of split window algorithms for land surface temperature retrieval from NOAA-AVHRR data. In IGARSS 2004. 2004 IEEE International Geoscience and Remote Sensing Symposium 6:3740–3743
- Rajeshwari A and Mani N D 2014 Estimation of land surface temperature of Dindigul district using Landsat 8 data *International Jour Res Engg Tech* v3 (5) pp122-126
- Raynolds MK, Comiso JC, Walker DA, Verbyla D (2008) Relationship between satellite-derived land surface temperatures, arctic vegetation types, and NDVI. *Remote Sens Environ* 112(4):1884–1894
- Rouse JW, Haas RH, Schell JA, Deering DW, Harlan JC (1974) Monitoring the vernal advancement and retrogradation of natural vegetation. In: NASA/GSFC, Type III. Final report, Greenbelt MD, pp 1–371
- Salereo F, Gaetano V, Gianni T (2018) Urbanization and climate change impacts on surface water quality: enhancing the resilience by reducing impervious surfaces CNR – Water Research Institute. IRSA
- Salih MM, Jasim OZ, Hassoon KI, Abdalkadhum AJ (2018) Land surface temperature retrieval from LANDSAT-8 thermal infrared sensor data and validation with infrared thermometer camera. *International Journal of Eng Technol* 7(4.20):608–612
- Sayão VM, Demattê JA, Bedin LG, Nanni MR, Rizzo R (2018) Satellite land surface temperature and reflectance related with soil attributes. *Geoderma* 325:125–140
- Sayão VM, dos Santos NV, de Sousa Mendes W, Marques KP, Safanelli JL, Poppiel RR, Demattê JA (2020) Land use/land cover changes and bare soil surface temperature monitoring in southeast Brazil. *Geoderma Regional* 22:e00313
- Sekertekin A, Kutoglu SH, Kaya S, Marangoz AM (2015) Analysing the effects of different land cover types on land surface temperature using satellite data. *Int Arch Photogramm Remote Sens Spat Inf Sci* 40(1):665
- Shalaby A, Tateishi R (2007) Remote sensing and GIS for mapping and monitoring land cover and land-use changes in the Northwestern coastal zone of Egypt. *Appl Geogr* 27(1):28–41
- Shukla AK, Ahmad I, Verma MK (2021) Change detection analysis in L, use I, cover pattern with the integration of remote sensing, GIS techniques. *International Research Journal of Modernization in Engineering Technology, Science* 3(9):1334–1338
- Simó G, García-Santos V, Jiménez MA, Martínez-Villagrasa D, Picos R, Caselles V, Cuxart J (2016) Landsat and local land surface temperatures in a heterogeneous terrain compared to modis values. *Remote Sens* 8(10):849
- Sinha S, Sharma LK, Singh Nathawat MS (2015) Improved Land-use/Land-cover classification of semi-arid deciduous forest landscape using thermal remote sensing. *Egypt J Remote Sens Space Sci* 18(2):217–233. <https://doi.org/10.1016/j.ejrs.2015.09.005>.
- Sinha J, Sahu RK, Agarwal A, Pali AK, Sinha BL (2013) Rainfall-Run off Modelling using Multi Layer Perceptron Technique-A Case Study of the Upper Kharun Catchment in Chhattisgarh. *Journal of Agricultural Engineering* 50(2):43–51
- Sobrino JA, Jiménez-Muñoz JC, Paolini L (2004) Land surface temperature retrieval from LANDSAT TM 5. *Remote Sens Environ* 90(4):434–440
- Spence M, Annez P, Buckley R (2009) Urbanization and growth. World Bank, Washington, DC, USA
- Srivastava PK, Majumdar TJ, Bhattacharya AK (2009) Surface temperature estimation in Singhbhum Shear Zone of India using Landsat-7 ETM+ thermal infrared data. *Adv Space Res* 43(10):1563–1574
- Srivastava PK, Majumdar TJ, Bhattacharya AK (2010) Study of land surface temperature and spectral emissivity using multi-sensor satellite data. *J Earth Syst Sci* 119:67–74
- Sun D, Kafatos M (2007) Note on the NDVI-LST relationship and the use of temperature-related drought indices over North America. *Geophys Res Lett* 34(24)
- Tsou J, Zhuang J, Li Y, Zhang Y (2017) Urban heat island assessment using the Landsat 8 data: a case study in Shenzhen and Hong Kong. *Urban Sci* 1(1):10
- Tucker CJ, Sellers PJ (1986) Satellite remote sensing of primary production. *Int J Remote Sens* 7(11):1395–1416
- Vellaiyan G, Chokkalingam L, Ramki P (2017) Visual interpretation methods of land use/land cover changes and analysis using Gis & remote sensing technology: a case study of Gomukhi River Basin of Tamil Nadu India International. *J Adv Res* 5:638–649. <https://doi.org/10.21474/Ijar01/5101>
- Verma P, Raghubanshi AS (2019) Rural development and land use land cover change in a rapidly developing agrarian South Asian landscape. *Remote Sensing Applications: Society and Environment* 14:138–147
- Vlassova L, Perez-Cabello F, Nieto H, Martín P, Riaño D, de la Riva J (2014) Assessment of methods for land surface temperature retrieval from Landsat-5 TM images applicable to multiscale tree-grass ecosystem modeling. *Remote Sens* 6:4345–4368
- Wan Z (2007) Collection-5 MODIS land surface temperature products users' guide. University of California, Santa Barbara, ICES
- Weng QH, Lu DS, Schubring J (2004) Estimation of land surface temperature vegetation abundance relationship for urban heat island studies. *Remote Sens Environ* 89(4):467–483
- Xiao H, Weng Q (2007) The impact of land use and land cover changes on land surface temperature in a karst area of China. *J Environ Manag* 85(1):245–257
- Yang Y, Huang S (2014) Suitability of five cross validation methods for performance evaluation of nonlinear mixed-effects forest models—a case study. *Forestry: An International Journal of Forest Research* 87(5):654–662
- Yuan F, Bauer ME (2007) Comparison of impervious surface area and normalized difference vegetation index as indicators of surface urban heat island effects in Landsat imagery. *International Journal of Remote Sensing of Environment* 106:375–386
- Yue W, Xu J, Tan W, Xu L (2007) The relationship between land surface temperature and NDVI with remote sensing: application to Shanghai Landsat & ETM+ data. *Int J Remote Sens* 15:3205–3226
- Zha Y, Gao J, Ni S (2003) Use of normalized difference built-up index in automatically mapping urban areas from TM imagery. *Int J Remote Sens* 24(3):583–594. <https://doi.org/10.1080/01431160304987>
- Zhang H, Jin MS, Leach M (2017) A study of the oklahoma city urban heat island effect using a wrf/single-layer urban canopy model a joint urban 2003 field campaign and modis satellite observations. *Climate* 5(3):72

**Publisher's note** Springer Nature remains neutral with regard to jurisdictional claims in published maps and institutional affiliations.

Springer Nature or its licensor (e.g. a society or other partner) holds exclusive rights to this article under a publishing agreement with the author(s) or other rightsholder(s); author self-archiving of the accepted manuscript version of this article is solely governed by the terms of such publishing agreement and applicable law.